remote sensing

Article

Mapping Grassland Classes Using Unmanned Aerial Vehicle and MODIS NDVI Data for Temperate Grassland in Inner Mongolia, China

Baoping Meng [1,2], Yuzhuo Zhang [1,2], Zhigui Yang [1,2], Yanyan Lv [1,2], Jianjun Chen [3], Meng Li [1,2], Yi Sun [1,2], Huifang Zhang [1,2], Huilin Yu [1,2], Jianguo Zhang [1,2], Jie Lian [4], Mingzhu He [4], Jinrong Li [5], Hongyan Yu [6], Li Chang [7] and Shuhua Yi [1,2,*]

[1] Institute of Fragile Eco-Environment, Nantong University, Nantong 226007, China; mengbp09@lzu.edu.cn (B.M.); 1822021005@stmail.ntu.edu.cn (Y.Z.); 1822021025@stmail.ntu.edu.cn (Z.Y.); lvyy09@lzu.edu.cn (Y.L.); limeng@ntu.edu.cn (M.L.); sunyi@ntu.edu.cn (Y.S.); zhf10658@ntu.edu.cn (H.Z.); 2017320004@stmail.ntu.edu.cn (H.Y.); 2021110030@stmail.ntu.edu.cn (J.Z.)
[2] School of Geographic Science, Nantong University, Nantong 226007, China
[3] College of Geomatics and Geoinformation, Guilin University of Technology, Guilin 541004, China; chenjj@lzb.ac.cn
[4] Northwest Institute of Eco-Environment and Resources, Chinese Academy of Sciences, Lanzhou 730000, China; lianjie@lzb.ac.cn (J.L.); hmzecology@lzb.ac.cn (M.H.)
[5] Yinshanbeilu National Field Research Station of Desert Steppe Eco-Hydrological System, Institute of Water Resources and Hydropower Research, Beijing 100038, China; lijinrong918@126.com
[6] Qinghai Service and Guarantee Center of Qilian Mountain National Park, Xining 810001, China; 18909718038@189.cn
[7] College of Urban Environment, Lanzhou City University, Lanzhou 730070, China; changli@lczu.edu.cn
* Correspondence: yis@ntu.edu.cn

Citation: Meng, B.; Zhang, Y.; Yang, Z.; Lv, Y.; Chen, J.; Li, M.; Sun, Y.; Zhang, H.; Yu, H.; Zhang, J.; et al. Mapping Grassland Classes Using Unmanned Aerial Vehicle and MODIS NDVI Data for Temperate Grassland in Inner Mongolia, China. *Remote Sens.* **2022**, *14*, 2094. https://doi.org/10.3390/rs14092094

Academic Editors: Anna Jarocińska, Adriana Marcinkowska-Ochtyra and Adrian Ochtyra

Received: 18 March 2022
Accepted: 25 April 2022
Published: 27 April 2022

Abstract: Grassland classification is crucial for grassland management. One commonly used method utilizes remote sensing vegetation indices (VIs) to map grassland classes at various scales. However, most grassland classifications were conducted as case studies in a small area due to lack of field data sources. At a small scale, classification is reliable; however, great uncertainty emerges when extended to other areas. In this study, large amounts of field observations (more than 30,000 aerial photos) were obtained using unmanned aerial vehicle photography in Inner Mongolia, China, during the peak period of grassland growth in 2018 and 2019. Then, four machine learning classification algorithms were constructed based on characteristic indices of MODIS NDVI in the growing season to map grassland classes of Inner Mongolia. Finally, the spatial distribution and temporal variation of temperate grassland classes were analyzed. Results showed that: (1) Among all characteristic indices, the maximum, average, and sum of MODIS NDVI from July to September during 2015 to 2019 greatly affected grassland classification. (2) The random forest method exhibited the best performance with overall accuracy and kappa coefficient being 72.17% and 0.62, respectively. (3) Compared with the grassland class mapped in the 1980s, 30.98% of grassland classes have been transformed. Our study provides a technological basis for effective and accurate classification of the temperate steppe class and a theoretical foundation for sustainable development and restoration of the temperate steppe ecosystem.

Keywords: temperate steppe; grassland classification; MODIS NDVI; spatial variation

1. Introduction

Grassland classification is crucial for grassland management, which formulates classes through grouping or clustering with similar properties [1–3]. The grassland classes provide the basis for the utilization and protection of grassland resources and the principle for the reconstruction and restoration of a grassland ecological environment [4–8]. As an essential component of the Eurasian steppe, the temperate steppe is one of the extensive grasslands in China and is primarily distributed on the Inner Mongolian Plateau [9]. The temperate steppe provides necessary resources for the development of animal husbandry in the pastoral areas of northern China. It is also an important natural buffer that provides ecological environment protection in northern China [9,10]. However, due to the climate change and anthropogenic activities [9,11,12], Inner Mongolian grassland classes experienced rapid transformation during the lasted four decades [13–15]. The grassland classes need to be updated to improve the understanding and management of temperate steppe ecosystems.

Traditional grassland classes were visually interpreted based on field surveys and remote sensing images at large scales [16,17]. The main limitations of the traditional classification approach include: (1) low efficiency, requiring large amounts of labor, cost, and resources; (2) difficulty in monitoring the dynamic variation of grassland classes at large scales in the long term; and (3) large uncertainty brought by subjective biases of different investigators in class mapping [18,19]. For example, to clarify the situation of grassland resources in China, the 1:10 million China grassland resource (including grassland classes) was mapped based on field investigation and measurement and assisted by satellite and aerial image verification in the 1980s [20]. The map was produced by a large group of scientists for over a decade. Since its publication, it has been used as a fundamental input for policy making and ecological studies [20]. However, the map of grassland resources has not been updated yet in the last four decades, and the current situation of grassland resources cannot be accurately reflected.

The development of remote sensing technology has provided the possibility of monitoring landscape and different vegetation biomes, such as agricultural plants [21,22], forests, [23] and grasslands [24], and creating land-use/land-cover maps with a high efficiency [25–27]. MODIS data have both a high temporal resolution (daily) and a broad spatial coverage compared with high-resolution satellite images. Those features are suitable for monitoring grassland dynamic changes at a large scale [28,29]. Researchers have widely used a combination of MODIS NDVI data with different machine learning approaches to classify grasslands worldwide [30–34]. However, limited by time, labor, cost, and resources, the large-scale field investigation is still a great challenge for scientists [35,36]. The classification of grassland classes mainly focuses on the case studies in small areas. At a small scale, classification is reliable; however, great uncertainty emerges when extended to other areas [37,38].

The recently developed unmanned aerial vehicle (UAV) technology has received much of attention in grassland resource monitoring, which has overcome the shortcoming of satellite and traditional methods [35,39,40]. UAV provides a wide range of high-resolution aerial photographs, which obtain vegetation information effectively at the site scale [41]. UAV is easy to operate and saves time and effort [39]. Yi et al. (2017) [34] developed a set of UAV aerial photography systems with fixed-point, multisite, collaborative monitoring over large regions. Machine learning algorithms (e.g., gradient boosting decision tree (GBDT) and random forest (RF) [10,38]) have been widely used in remote sensing vegetation classification due to their powerful adaption, self-learning, and parallel processing capabilities [11,38,39].

In this study, we aimed to map the grassland classes of a temperate steppe in Inner Mongolia using the combination of UAV aerial photographs, MODIS NDVI, and machine learning algorithms to clarify the spatial differentiation and variation (compared with the 1980s) of grassland classes. We hope this study can be helpful for exploring the impact of climate change and anthropogenic activities on grassland vegetation and providing a theoretical basis for the sustainable development of grassland in Inner Mongolia.

2. Data and Methods

2.1. Study Area

The temperate grassland of Inner Mongolia is an important part of the Eurasian steppe (97°12′–126°04′E, 37°24′–53°23′N), with an area of 0.88 $\times$ 10^6 km^2 (2400 km from east to west, 1700 km from north to south) [15]. The elevation of Inner Mongolia is between 1000 and 3000 m (Figure 1b). It belongs to the continental monsoon climate, with uneven distribution of precipitation and temperature. The annual average temperature is −5–10 °C, increasing from northeast to southwest. The precipitation ranges from 35 mm to 530 mm, decreasing from northeast to southwest. The grassland classes of Inner Mongolia mainly include temperate meadow steppe (TMS), temperate typical steppe (TTS), temperate desert steppe (TDS), temperate steppe desert (TSD), and temperate desert (TD) from northeast to southwest (Figure 1a). Besides, the mountain meadow and lowland meadow were distributed in the northeast of the study area, and swamp meadow was scattered in the whole study area. The areas of those classes were relatively small.

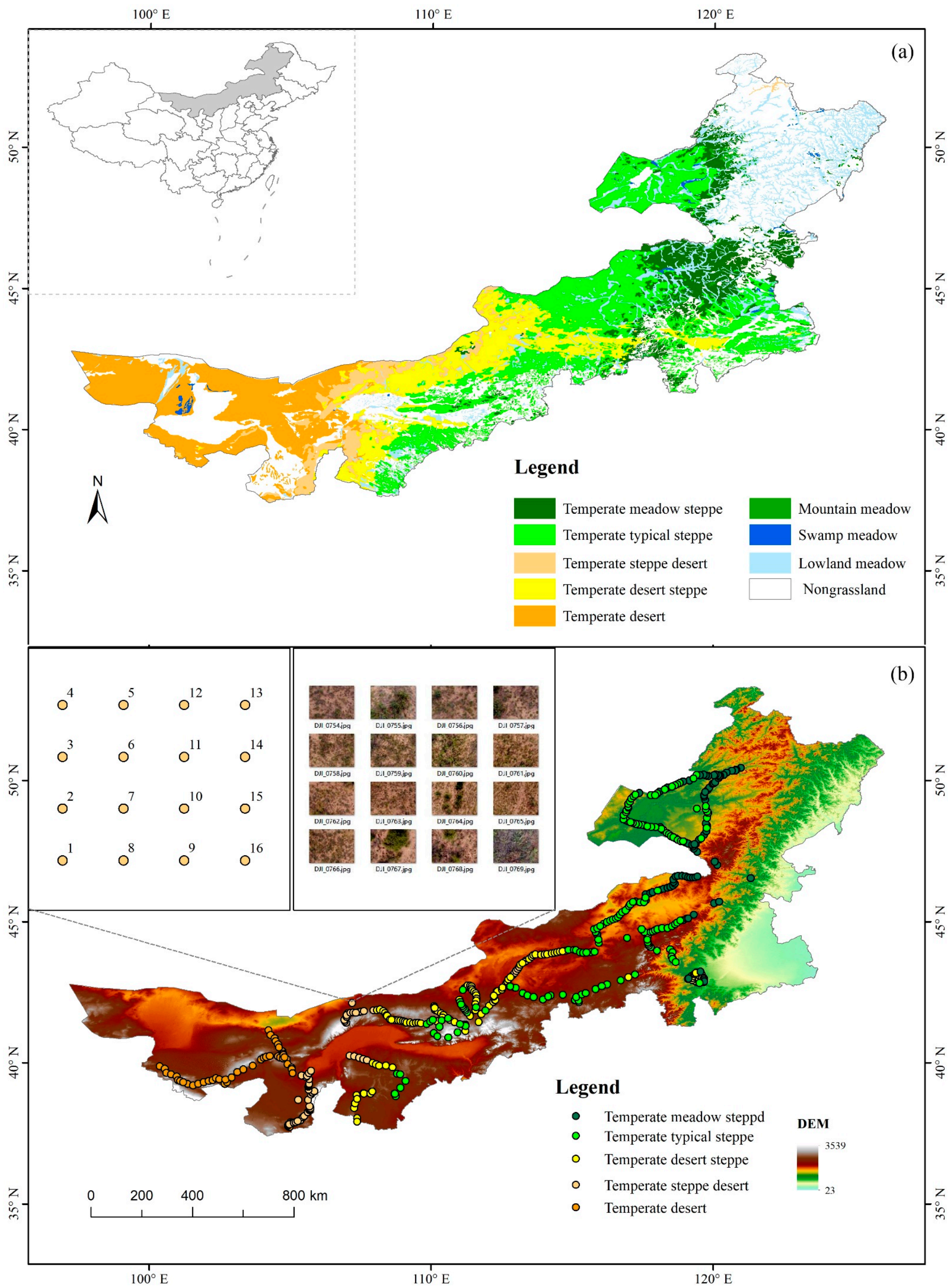

Figure 1. Grassland classes (in the 1980s) (**a**) and observation sites with UAV in Inner Mongolia, China (**b**).

2.2. Field Observation

In this study, we carried out the field observation for grassland class based on aerial photographs by Phantom 3 Professional and Mavic 2 Zoom Quad-Rotor intelligent UAVs (manufactured by DJI Innovation Industries; http://www.dji.com (accessed on 17 March 2022)), and grassland classes were retrieved from aerial photographs. According to the vegetation of grassland classes and spatial representativeness, a 250 m × 250 m area was selected as an observation site (corresponding to one MODIS pixel). Four flight routes were designed for each site, including one GRID route (200 m × 200 m) and three BELT routes (40 m × 40 m) (Figure 2). FragMAP was used to set up and execute the flight routes [35]. Phantom 3 Professional was used to perform the GRID flight route at a height of 20 m (red dots in Figure 2a,b), and Mavic 2 Zoom was used to perform the BELT flight route at a height of 2 m (green dots in Figure 2a,c). The positional accuracy of the two UAVs was ±1.5 m horizontally and ±0.5 m vertically. Sixteen photographs were then taken vertically downward at each waypoint automatically. The photograph resolutions of GRID and BELT are 1 cm and 0.09 cm, and the ground coverages are 26 m × 35 m and 3.43 m × 2.57 m, respectively. Field observations were carried out at the peak time of grassland growth (July to August). According to the distribution of grassland classes in Inner Mongolia, the observation sites were set up along the major traffic roads and areas accessible by vehicles. The observation sites were as evenly distributed as possible, with ~10 km distance between each other. Additionally, 797 observation sites were investigated from 2018 to 2019 in total (Figure 1b).

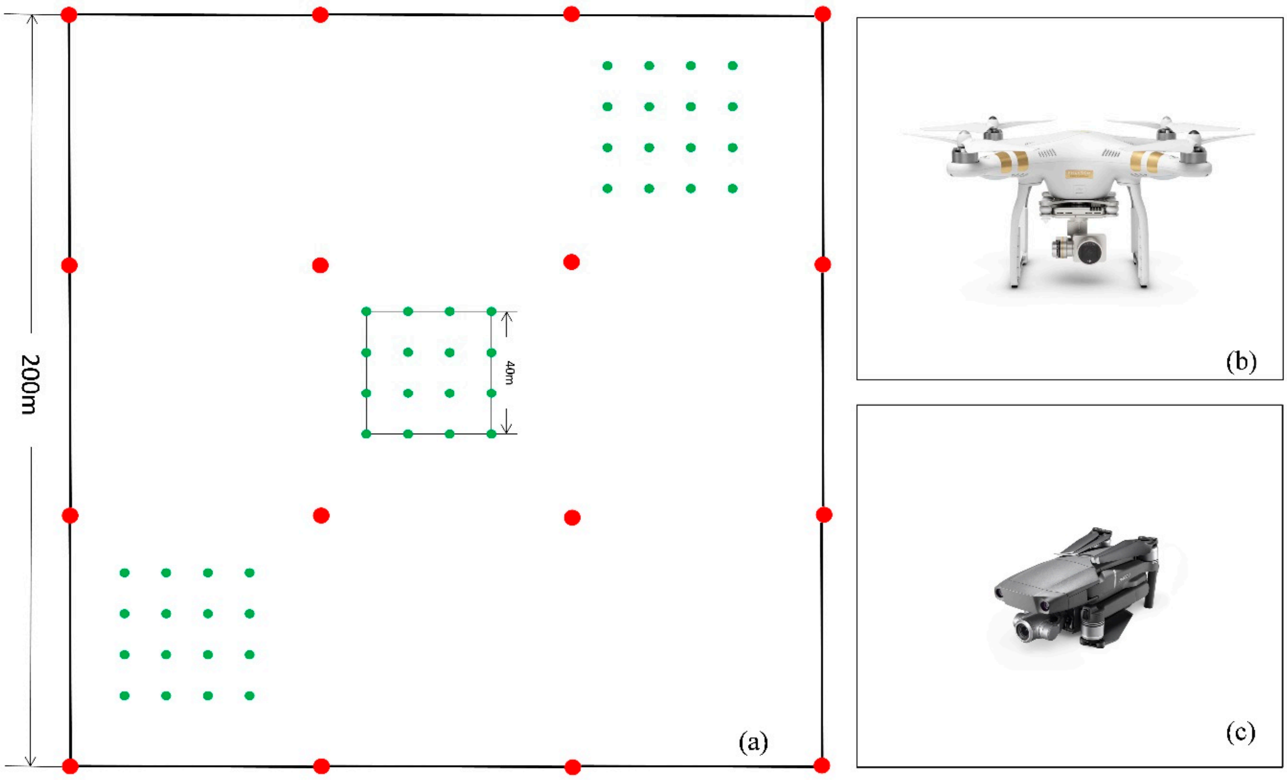

Figure 2. Strategy of field observation and data collection: (**a**) strategy of observation site; (**b**,**c**) are Phantom 3 Professional and Mavic 2 Zoom Quad-Rotor intelligent UAVs.

2.3. Grassland Classification in Observation Sites

In this study, five major grassland classes (TMS, TTS, TDS, TSD, and TD) were observed in Inner Mongolia, China. The aerial photographs were divided into different grassland classes according to the vegetation life form, dominant grass species, and vegetation coverage (Figure 3 and Table 1). According to the GPS information recorded in

FragMAP and stored in aerial photographs' property files, the names of photographs were renamed as number 1 to 16 by the DJI Locator software in each site [34]. Then the remote sensing classification label was built based on photograph location information (in ArcGIS software).

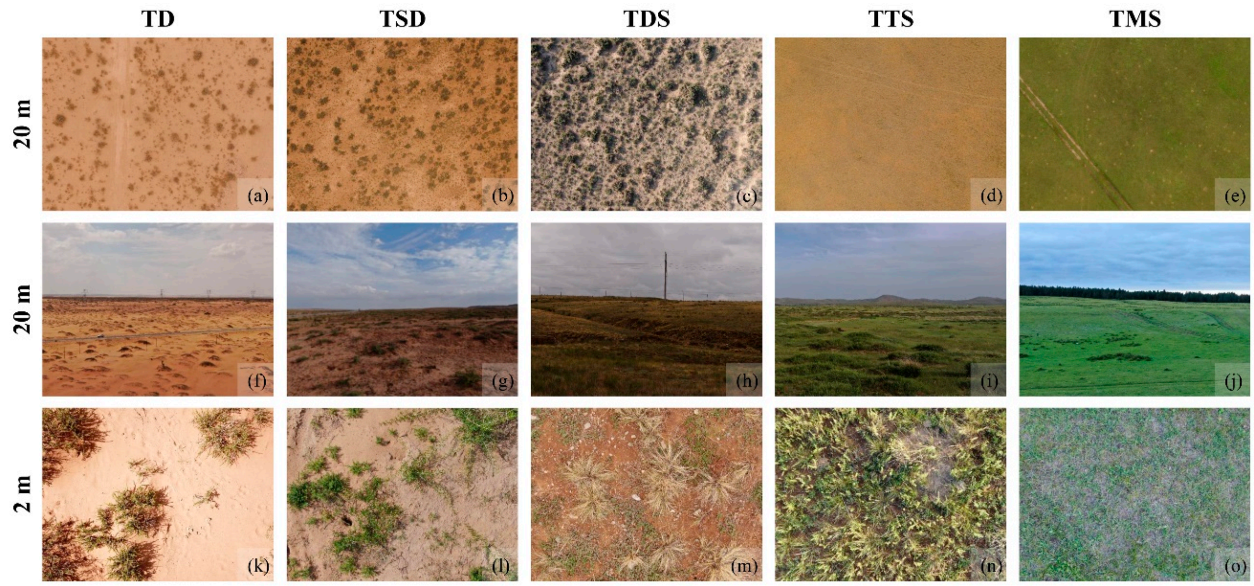

Figure 3. Aerial photographs of temperate steppe classes. (**a**–**j**) are aerial photographs taken at a height of 20 m by Phantom 3; (**a**–**e**) are taken vertically downward; (**f**–**j**) are taken tilted with 45 degrees; (**k**–**o**) are aerial photographs taken at a height of 2 m by Mavic 2, acquired with 2× wide-angle zoom lenses; TD, TSD, TDS, TTS, and TMS represent grassland classes of temperate desert, temperate steppe desert, temperate desert steppe, temperate typical steppe, and temperate meadow steppe, respectively.

Table 1. Characteristics of different grassland classes in temperate steppe.

Grassland Classes	Vegetation Life Form	Dominant Grass Species	Coverage
TD	Extremely xerophytic short shrubs, semishrubs	*Lyonia ovalifolia*, *Salsola laricifolia*, *Reaumuria songarica*, *Kalidium foliatum*, *Artemisia desertorum*, *Psammochloa villosa*	0–20%
TSD	Super xerophytic semi-shrubs, shrubs, and xerophytic grasses	*Seriphidium gracilescens*, *Seriphidium terrae-albae*, *Seriphidium borotalense*, *Sympegma regelii*, *Reaumuria soongorica*, *Anabasis brevifolia*, *Stipa glareosa*	20–30%
TDS	Super xerophytic grasses, xerophytic short/semishrubs	*Stipa tianschanica*, *Stipa breviflora*, *Cleistogenes songorica*, *Artemisia frigida*, *Allium mongolicum*, *Allium aflatunense*	30–40%
TTS	Xerophytic perennial tufted grasses, xerophytic short shrubs	*Stipa grandis*, *Stipa krylovii*, *Stipa bungeana*, *Cleistogenes squarrosa*, *Agropyron cristatum*, *Artemisia frigida*, *Caragana sinica*	60–70%
TMS	Mesoxerophytic perennial tufted grasses and root grasses	*Stipa baicalensis*, *Leymus chinensis*, *Filifolium sibiricum*	70–90%

TD, TSD, TDS, TTS, and TMS represent grassland classes of temperate desert, temperate steppe desert, temperate desert steppe, temperate typical steppe, and temperate meadow steppe, respectively.

2.4. Acquisition and Reprocessing of Remote Sensing Data

MODIS vegetation index production and MCD12Q1 land-cover data were obtained from the United States Geological Survey (USGS; https://e4ftl01.cr.usgs.gov/ (accessed on 17 March 2022)). The data of the MODIS vegetation index were selected from the MODIS 16-d maximum composite NDVI vegetation index product (MOD13Q1). In total, 60 images (the spatial resolution was 250 m, and the orbit numbers were h25v03, h25v04, h25v05, h26v03, h26v04, h26v05, and h27v04) were selected during the grassland growth season (May to September) from 2015 to 2019. The MOD13Q1 NDVI data were transformed and registered to an Albers projection with a Geo-Tiff format by using a MODIS reprojection tool (MRT). The Raster calculator module in ArcMap was employed to calculate the maximum, minimum, median, mean, range, standard deviation, and sum NDVI value from May to September during 2015 to 2019. A total of 35 indices were calculated to describe the characteristics of NDVI variation of grassland classes in the growing season.

The land cover was acquired from the IGBP global vegetation classification scheme (LC_type1, annual IGBP classification) dataset (MCD12Q1) with a spatial resolution of 500 m. In this study, the spatial distribution of grassland based on land cover in Inner Mongolia was obtained as the reclassification scheme of the Supplementary File.

2.5. Classification Methods

The decision tree (DT), gradient boosting decision tree (GDBT), random forest (RF), and logistic regression (LR) classification algorithms were employed in this study. The DT is a classification procedure that recursively partitions a data set into smaller subdivisions based on tests defined at each branch in the tree. It is classified by sequentially subdividing the target object according to the decision framework defined by the tree. Each observation's class label is assigned according to the leaf node with the observation falls [42]. GDBT combines decision tree and ensemble learning techniques, which generates a new decision tree by calculating the gradient (direction of residual error). Each iteration is carried out according to the direction of residual error reduction. Finally, several decision tree models are obtained. The prediction result is weighted by these several decision trees [43]. The RF algorithm applies a set of DTs to improve the prediction accuracy. We employed a bootstrap sample to construct a DT. Training samples were constantly selected to minimize the sum of the squared residuals until a complete tree was formed. A multiple DT was formed, and the voting was used to obtain the final prediction [44,45]. LR is a nonlinear classification method based on regression analysis of binary dependent variables (0 or 1). The relationship between characteristic variables and classification target was expressed by a regression equation through quantitative analysis between grassland classes and corresponding variables [46].

Four classification algorithms mentioned above were performed using Python in the Jupyter Notebook. The hyperparameters of DT, GDBT, and RF (including the number of estimators, maximum depth of the decision tree, minimum of leaf node samples, and so on) were determined based on a trial-and-error process [47,48]. The input data consisted of a training set and a validation set. The training set was used to adjust the weights on each algorithm, and the validation set was used to minimize overfitting. Training automatically stops when generalization stops improving, as indicated by the stopped-decreasing or even-increasing accuracy between the measured values and model outputs in the validation samples. In this study, the ID3 algorithm was selected for training the classification; by combining the different hyperparameters, we constructed the grassland classes' classification methods.

2.6. Variables Selection and Accuracy Validation

To reduce the influence of self-correlation and information redundancy, all factors were screened by importance value before building the classification model. The leave-one-out-cross-validation (LOOCV) method was used to calculate the importance value for each variable (Equation (1)). The cumulative contribution of each variable was calculated based on the importance value, and the variables with a cumulative contribution higher than or equal to 85% were selected as the input data of remote sensing classification. The equation for importance value is:

$$\text{Importance} = 1 - \text{cor (pred\_ref, pred\_shuffled)} \tag{1}$$

where ref is defined as a dataset that contains all variables, shuffled is defined as a dataset removing a single variable randomly, cor represents calculating the correlation coefficient, pred_ref represents the prediction based on a dataset containing all variables, and pred_shuffled represents the prediction based on a dataset removing a single variable.

In this study, the observed sites were divided into two parts. About 70% of the sites were randomly selected as a training set, and the rest were used to validate classification accuracy. The standard confusion matrix was employed to evaluate the classification accuracy of images. The accuracy evaluation index included the overall accuracy (OA), kappa coefficient (Kappa), user's accuracy (UA), and producer's accuracy (PA).

$$\text{OA} = \frac{\sum_{i=1}^{r} x_{ii}}{N} \tag{2}$$

$$\text{Kappa} = \frac{N\sum_{i=1}^{r} x_{ii} - \sum_{i=1}^{r}(x_{i+} \times x_{+i})}{N^2 - \sum_{i=1}^{r}(x_{i+} \times x_{+i})} \tag{3}$$

$$\text{PA}_i = \frac{x_{ii}}{x_{+i}} \tag{4}$$

$$\text{UA}_i = \frac{x_{ii}}{x_{i+}} \tag{5}$$

where N represents the number of validation sites, n_{ii} represents the number of validation sites for correct classification, x_{+i} represents the number of validation sites classified to the same grassland class, x_{i+} represents the number of validation sites that belong to the same grassland class, and r represents the number of grassland classes.

3. Results

3.1. Characteristics of Field Observation and Corresponding NDVI

The distribution of observed sites is shown in Figure 1b. The grassland classes showed a regular spatial distribution in Inner Mongolia, which presented as TMS, TTS, TDS, TSD, and TD from northeast to southwest. The number of TTS observation sites was largest, accounting for 33.61% of all observation sites, followed by TDS, TMS, TSD, and TD, with percentages ranging from 11.75% to 24.74%. The characteristic indices of growing season NDVI are shown in Figure 4. Among the five grassland classes, the NDVI characteristic indices of TMS had a higher value and the highest difference, followed by TTS, TDS, and TSD. The NDVI characteristic indices of TD had lower values and the lowest difference. The mean and median values were similar with little difference during the grassland growing season (from May to September during 2015–2019). All index values were higher in August and September than in other months.

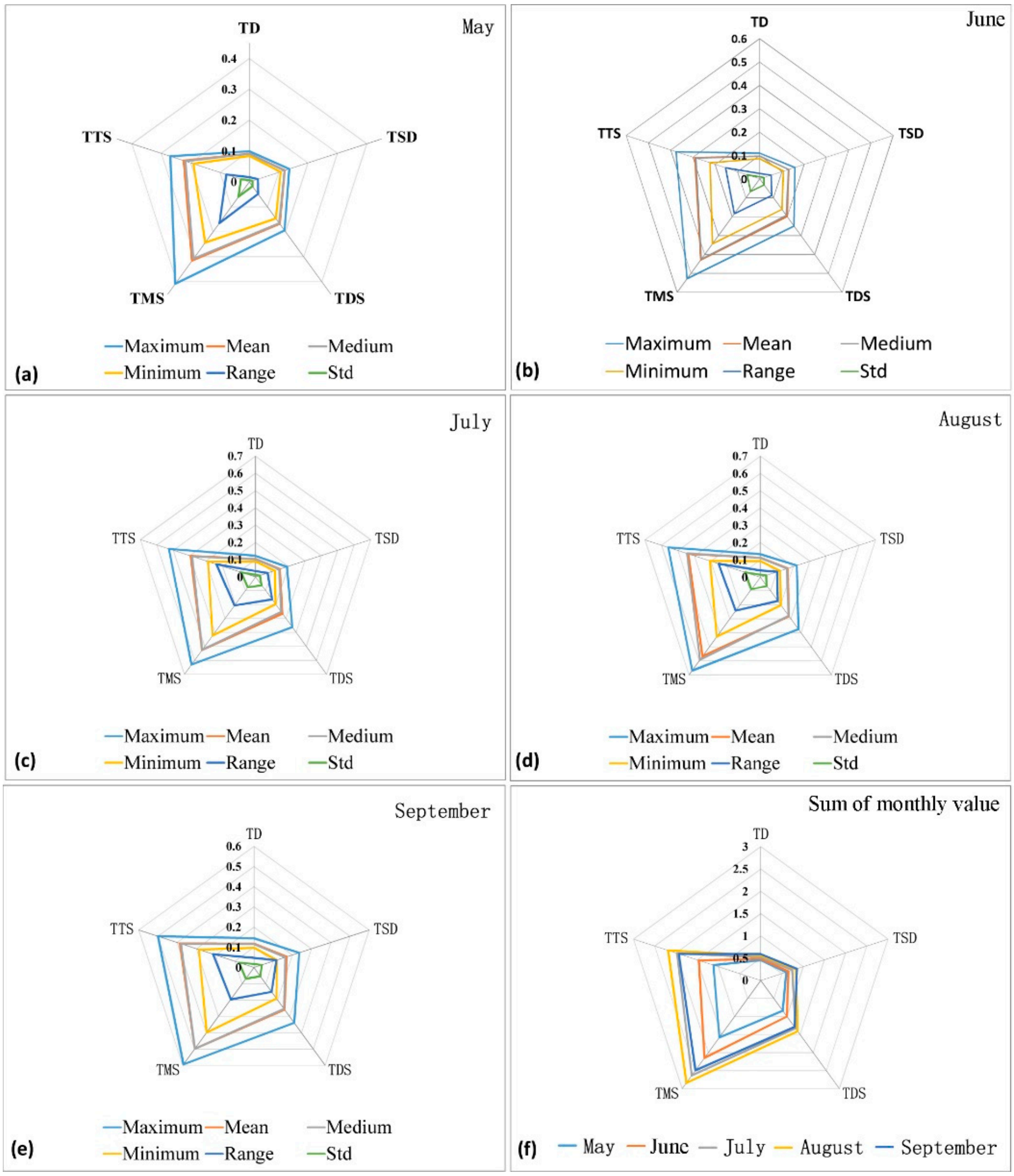

Figure 4. The characteristics of growing season (May to September) NDVI during 2015 to 2019 (**a**–**e**) were maximum, mean, median, minimum, range, and standard deviation of monthly multiyear NDVI; (**f**) was the sum of monthly multiyear NDVI; TMS, TTS, TDS, TSD, and TD were temperate meadow steppe, temperate typical steppe, temperate desert steppe, temperate steppe desert, and temperate desert, respectively.

3.2. Selection of NDVI Characteristic Indices

The importance values and cumulative contribution of different NDVI characteristic indices (calculated by Pearson coefficient) were exhibited in Table 2. There were 11 indices with importance values higher than 3%. Additionally, the cumulative contribution reached 51.02%, including the maximum, mean, and sum of NDVI in September and July; sum, mean, and median of NDVI in August; and maximum and mean of NDVI in June. There were 12 indices with importance values between 2% and 3%, including median and minimum of NDVI in September and July; maximum of NDVI in August; sum, median, and minimum of NDVI in June; and mean, maximum, median, and sum of NDVI in May.

The importance values for rest indices were less than 2%, mainly including the range and standard deviation of NDVI from May to September. Among all indices, the cumulative contribution of the first 25 indices reached 85%.

Table 2. Importance and cumulative contribution of NDVI characteristics indices.

Index	Importance (%)	Contribution (%)	Index	Importance (%)	Contribution (%)
Sum_8	7.58	7.58	Minimum_6	2.5	72.43
Mean_8	6.25	13.83	Median_5	2.27	74.71
Maximum_9	5.57	19.4	Minimum_9	2.21	76.92
Sum_7	5.28	24.68	Sum_5	2.1	79.02
Median_8	4.63	29.31	Minimum_7	2.04	81.06
Mean_7	4.34	33.65	Minimum_8	1.76	82.82
Mean_9	4.07	37.73	Std_6	1.75	84.57
Maximum_6	3.72	41.45	Std_9	1.73	86.3
Sum_9	3.22	44.67	Range_9	1.72	88.02
Maximum_7	3.22	47.88	Std_8	1.6	89.62
Mean_6	3.14	51.02	Range_5	1.6	91.22
Mean_5	2.93	53.95	Std_5	1.56	92.78
Mediam_9	2.8	56.76	Minimum_5	1.52	94.3
Sum_6	2.74	59.5	Range_6	1.51	95.81
Maximum_5	2.67	62.17	Std_7	1.48	97.29
Medium_7	2.66	64.82	Range_7	1.44	98.73
Maximum_8	2.59	67.41	Range_8	1.27	100
Median_6	2.52	69.93			

Note: The number 5–9 represent May to September; maximum, minimum, median, mean, range, std, and sum represent the characteristic indices of NDVI in May to September during 2015 to 2019; and std represents standard deviation.

3.3. Accuracy Evaluation of Classification Methods

Combined with the NDVI characteristic indices (screened in Section 3.2) and the observed grassland classes, the DT, GDBT, RF, and LR algorithms were used to train the classification model. The results of accuracy evaluation are shown in Table 3. The RF algorithm performed best among the four classification methods, with an overall accuracy of 72.17% and a kappa coefficient of 0.62, followed by LR (OA of 69.81%, kappa of 0.58) and GDBT (OA of 69.34%, kappa of 0.58). The accuracy of DT was lowest with OA and kappa of 62.74% and 0.63, respectively. Among the five grassland classes, TD had the highest PA and UA, followed by TDS, TTS, and TMS. The PA and UA of TSD were lowest in the four classification methods, with 61.54% to 90.91% and 35.71% to 53.33%, respectively.

Table 3. Accuracy of five grassland classes based on decision tree (DT), gradient boosting decision tree (GDBT), random forest (RF), and logistic regression (LR) in Inner Mongolia.

Grassland Classes	DT (%)		GDBT (%)		RF (%)		LR (%)	
	PA	UA	PA	UA	PA	UA	PA	UA
TMS	73.91	68.69	56.82	71.43	62.16	65.71	67.65	65.71
TTS	71.63	81.87	77.50	69.66	75.56	76.40	71.13	77.53
TDS	72.90	69.64	62.50	77.78	66.67	75.56	64.00	71.11
TSD	61.54	53.33	80.00	42.86	87.50	50.00	90.91	35.71
TD	90.91	76.92	76.47	86.67	77.78	93.33	70.00	93.33
OA (%)	62.74		69.34		72.17		69.81	
Kappa	0.63		0.58		0.62		0.58	

Note: overall accuracy, OA; producer's accuracy, PA; user's accuracy, UA; decision tree, DT; gradient boosting decision tree, GDBT; random forest, RF; logistic regression, LR; temperate meadow steppe, TMS; temperate typical steppe, TTS; temperate desert steppe, TDS; temperate steppe desert, TSD; temperate desert, TD.

The confusion matrix of five grassland classes based on the RF algorithm is shown in Table 4. The TD performed best in five grassland classes, with a PA of 77.78% and a UA of 93.33%. Of the validation samples, 22.22% were misclassified as TSD. The PA and UA of TMS were 62.16% and 65.71%, and about 32.43%, 2.70%, and 2.70% of the validation samples were misclassified as TD, TDS, and TSD, respectively. The PA and UA of TTS and TDS were similar (75.56%, 76.40% vs. 66.67%, 75.56%); 13.33%, 10.00%, and 1.11% of the TTS validation samples were misclassified as TMS, TDS, and TSD; and 17.65% and 15.68% of the TDS validation samples were misclassified as TTS and TSD. Among all grassland classes, the PA of TSD was highest with 87.50%, but the UA was lowest with 50.00%, and 12.50% of the validation samples were misclassified as TDS and TD (6.25% for each).

Table 4. The confusion matrix of the five grassland classes based on the RF algorithm.

Grassland Classes	Validation Dataset					Total	UA (%)
	TMS	TTS	TDS	TSD	TD		
TMS	23	12 (13.33%)	0	0	0	35	65.71
TTS	12 (32.43%)	68	9 (17.65%)	0	0	89	76.40
TDS	1 (2.70%)	9 (10.00%)	34	1 (6.25%)	0	45	75.56
TSD	1 (2.70%)	1 (1.11%)	8 (15.68%)	14	4 (22.22%)	28	50.00
TD	0	0	0	1 (6.25%)	14	15	93.33
Total	37	90	51	16	18	212	
PA (%)	62.16	75.56	66.67	87.50	77.78		

Note: producer's accuracy, PA; user's accuracy, UA; temperate meadow steppe, TMS; temperate typical steppe, TTS; temperate desert steppe, TDS; temperate steppe desert, TSD; temperate desert, TD.

3.4. Distribution of Grassland Classes in Inner Mongolia

The grassland classes of temperate steppe in Inner Mongolia were inversed by the RF classification algorithm based on characteristic indices of the growing season NDVI (with cumulative contribution reaching 85%). The distribution of the grassland classes in Inner Mongolia is shown in Figure 5. The TMS was mainly located in the northeast of Inner Mongolia (the mideast area of Hulunbeier, most of the Hinggan League, eastern Xilingol League, northwestern Tongliao and Chifeng, local area of Ulanqab, Hohhot, and Ordos) with an area of 16.28×10^4 km^2 (17.57% of the total grassland area). The TTS was mainly located in southeastern Inner Mongolia (western Hulunbeier, eastern Xilingol League, most area of Chifeng, Tongliao, and Hohhot) with an area of 28.52×10^4 km^2 (30.77% of the total grassland area). The TDS was mainly located in central Inner Mongolia (western Xilingol League, northern Ulanqab and Baotou, most areas of Ordos, and eastern of Bayannur) with an area of 18.89×10^4 km^2 (20.38% of the total grassland area). The TD was mainly located in western Inner Mongolia (almost all of the Alxa League and western Bayannur) with an area of 23.34×10^4 km^2 (25.18% of the total grassland area). Among all the grassland classes, the area of the TSD was smallest, with an area of 5.65×10^4 km^2 (6.1% of the total grassland area), mainly located in the transition zone of TDS to TD.

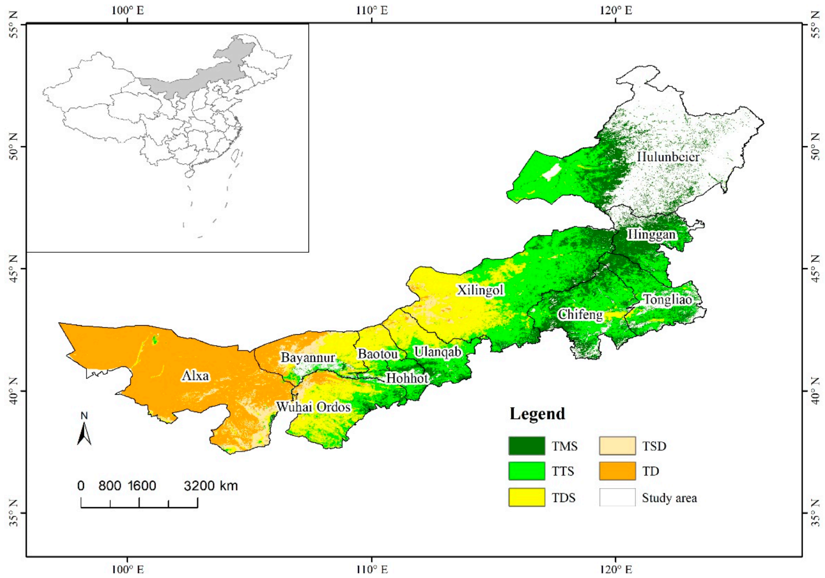

Figure 5. Spatial pattern of the grassland classes in Inner Mongolia. TD, TSD, TDS, TTS, and TMS represent the grassland classes of temperate desert, temperate steppe desert, temperate desert steppe, temperate typical steppe, and temperate meadow steppe, respectively.

3.5. Spatial and Temporal Variation of Grassland Classes in Inner Mongolia

In order to explore the variation of grassland classes in Inner Mongolia, the transition matrix was analyzed based on the overlapped region of grassland between the 1980s and this study (Figure 6, Tables 5 and 6). Compared with the grassland classes in the 1980s, the areas of TDS and TMS in 2019 increased by 0.57×10^4 km^2 and 3.87×10^4 km^2 (0.91% and 6.15% of overlapped grassland area), respectively. The areas of TSD, TTS, and TD decreased by 0.29×10^4 km^2, 3.93×10^4 km^2, and 0.22×10^4 km^2 (0.45%, 6.25%, and 0.36%), respectively (Tables 5 and 6). About 69.02% of overlapped grassland classes were unchanged. The spatial distribution of transitions is shown in Figure 6.

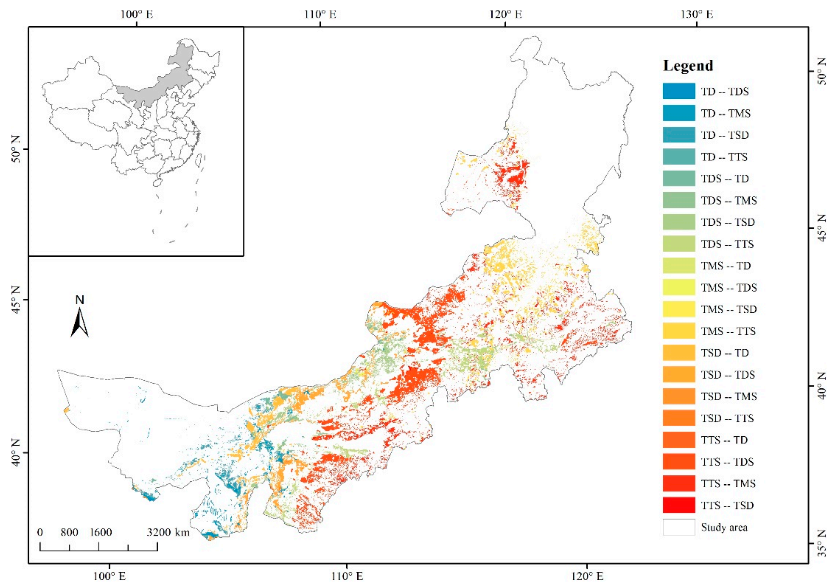

Figure 6. Spatial and temporal variation of grassland classes in Inner Mongolia (compared with an overlapped part of grassland in the 1980s); TD, TSD, TDS, TTS, and TMS represent grassland classes of temperate desert, temperate steppe desert, temperate desert steppe, temperate typical steppe, and temperate meadow steppe, respectively.

Table 5. Transition matrix of grassland glasses between the 1980s and 2019 ($\times 10^4$ km^2).

Transition Matrix	Grassland Classes in 2019							
	Grassland Classes	**TMS**	**TTS**	**TDS**	**TSD**	**TD**	**Total**	**Decrease**
Grassland classes in the 1980s	TMS	4.81	2.60	0.05	0.02	0.02	7.51	2.70
	TTS	3.08	14.02	5.27	0.07	0.01	22.46	8.43
	TDS	0.16	1.70	8.31	1.36	0.34	11.87	3.56
	TSD	0.01	0.08	1.76	1.94	1.17	4.96	3.02
	TD	0.01	0.13	0.34	1.28	14.30	16.06	1.76
	Total	8.07	18.53	15.74	4.67	15.83	62.86	
	Increase	3.27	4.51	7.43	2.73	1.54		

Note: TD, TSD, TDS, TTS, and TMS represent the grassland classes of temperate desert, temperate steppe desert, temperate desert steppe, temperate typical steppe, and temperate meadow steppe, respectively.

Table 6. Transition matrix of grassland glasses from the 1980s to 2019 (%).

Transition Matrix	Grassland Classes in 2019							
	Grassland Classes	**TMS**	**TTS**	**TDS**	**TSD**	**TD**	**Total**	**Decrease**
Grassland classes in the 1980s	TMS	7.65	4.14	0.08	0.03	0.03	11.94	4.29
	TTS	4.90	22.31	8.38	0.11	0.02	35.73	13.42
	TDS	0.26	2.70	13.22	2.16	0.54	18.89	5.66
	TSD	0.01	0.12	2.81	3.09	1.86	7.89	4.80
	TD	0.02	0.20	0.55	2.03	22.75	25.55	2.80
	Total	12.85	29.48	25.04	7.44	25.20	100	
	Increase	5.20	7.17	11.82	4.34	2.45		

Note: TD, TSD, TDS, TTS, and TMS represent the grassland classes of temperate desert, temperate steppe desert, temperate desert steppe, temperate typical steppe, and temperate meadow steppe, respectively.

In terms of the area transfer of grassland classes in the study area from 1980 to 2019 (Tables 5 and 6), TTS had the largest decreased area (13.42%), with 3.08 $\times$ 10^4 km^2, 5.27 $\times$ 10^4 km^2, 0.07 $\times$ 10^4 km^2, and 0.01 $\times$ 10^4 km^2 transferred into TMS, TDS, TSD, and TD, respectively. TDS had the largest increased area (11.82% of overlapped grassland area), with 0.05 $\times$ 10^4 km^2, 5.27 $\times$ 10^4 km^2, 1.76 $\times$ 10^4 km^2, and 0.34 $\times$ 10^4 km^2 transferred from TMS, TTS, TSD, and TD, respectively. The decreased and increased areas of TMS, TSD, and TD were similar.

4. Discussion

4.1. Remote Sensing Classification of Grassland Classes

Grassland classes are crucial for managing and utilizing grassland resources [1,5]. It is also vital for reconstructing and restoring the grassland ecological environment [4,6]. Due to a lack of reliable field observations, the spatial distribution and its variation are difficult to monitor. Most grassland class labels were obtained from field observation, expert knowledge, and literature review [11]. Previous field surveys were carried out at the scale of quadrat (1 $\times$ 1 m^2), plot, or transect (~100 $\times$ 100 m^2) [49]. It is impossible to complete the field surveys in the short term, because of the complexity and extensive spatial distribution of natural grassland resources. Meanwhile, expert knowledge and literature reviews cannot meet the accuracy requirement of classification, because of the subjective bias, the dynamic climate, and anthropogenic activities [29,39].

In this study, field observation was performed by UAV based on FragMAP [34,35]. Compared with traditional field survey methods, the UAV observation can cover a larger area. The area of aerial photographs taken by Phantom 3 at a height of 20 m was 35 m $\times$ 26 m, which was close to the traditional ground observation plot [39,50]. The range of observation can be further improved by the GRID flight route (extended to 250 m $\times$ 250 m), corresponding to one MODIS pixel. The resolution of Phantom 3 photographs at a height of 20 m is 0.87 cm. Combining the photographs taken by Mavic 2 at a height of 2 m (0.09 cm of resolution and

3.43 m × 2.57 m of covers), the grassland classes can be accurately identified [39,41,51]. Moreover, the UAV observations were more convenient and efficient. In this study, GRID and BELT routes can be performed simultaneously (about 15 min to finish each observation site), which provides the possibility for rapid observation in large regions [39]. Most importantly, once established, the flight routes and waypoints can be stored in FragMAP and used repeatedly (the error of two flights of the same waypoint is 1–2 m, and two photos on the same waypoint from two different flights of the GRID route are almost overlapped). It is suitable for monitoring the dynamic variation of grassland classes over a long-term period [35,40,52].

The classification algorithms and input indices also have a great impact on the accuracy of grassland classification [39]. Visual interpretation and unsupervised classification were mostly used in early grassland classification based on remote sensing data. The efficiency and accuracy of those methods cannot meet the requirements of grassland classification [10]. The development of remote sensing technology, with high temporal resolution and broad spatial coverage, provides the possibility for the map of grassland classes in an efficient and repeatable way [27]. Wen et al. (2010) [30] classified the grassland of Tibet into six classes based on the high temporal resolution of MODIS NDVI during the grass growth period in 2005. The overall accuracy was 68.02%, and kappa coefficient was 0.52. Zhang et al. (2011) [31] classified the grassland classes in the Wenquan area of Qinghai–Tibet Plateau based on MODIS EVI and field survey data. The overall accuracy and kappa coefficient were 72% and 0.6, respectively. Zhang et al. (2015) [32] divided the grassland in the Yili area of Xinjiang into seven classes based on MODIS NDVI and the decision tree classification algorithm. The overall accuracy was 68.45%, and the kappa coefficient was 0.52. The decision tree algorithm is the most used in the abovementioned studies, with a simple classification rule and low accuracy. In recent years, machine learning has been widely used in vegetation classification based on remote sensing data due to its high accuracy and powerful processing ability [38]. Our results also demonstrated that the RF algorithm had better performance than the other algorithms. The overall accuracy was increased by 4.92% to 7.90%, and kappa was increased by 0.1 to 0.18 compared with the abovementioned studies.

The index selection for training classification algorithms was based on important value and cumulative contribution (≥85%). In order to clarify the relationship between input index dataset and classification accuracy, the RF algorithm was used to perform the grassland classes' classification, and OA and kappa were used to evaluate the effects of different index combinations, which increased the indices according to the importance value from high to low, successively (Figure 7). With the increase in input indices, the variations of accuracy based on RF algorithms increased first and then stabilized. The lowest classification accuracy (OA and kappa were 62.94% and 0.52, respectively) was based on the input dataset consisting of one or two indices. The highest classification accuracy (OA and kappa were 76.92% and 0.70, respectively) was based on the first 25 indices, which was consistent with the results of the characteristic index selection in this study.

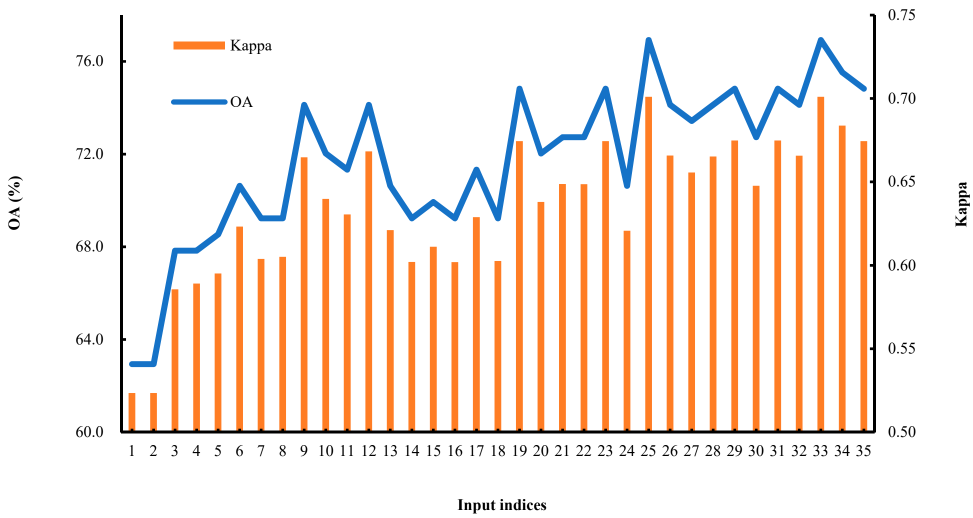

Figure 7. Variation of classification accuracy with the different input datasets based on RF algorithms.

4.2. Limitations and Prospects of Grassland Classification

In this study, although the optimum method for remote sensing monitoring of grassland classes in the study area was determined, some uncertainties regarding these classification algorithms remained due to limitations associated with various factors.

(1) Limitation in aerial photograph classification.

In this study, the observation sites were set along the main traffic route with an interval of 10–20 km in Inner Mongolia, and a total of 797 sites were observed from July to August in 2018 and 2019. Although the field observation based on UAV can improve efficiency and save cost and time, the grassland classes were mainly distinguished by visual interpretation (Figure 3 and Table 1). It was challenging to categorize a large number of aerial photographs (more than 30,000 aerial photos) into different grassland classes. It requires good knowledge of plant taxonomy and is time-consuming [11,39]. Hence, the automatic identification of vegetation classes based on aerial photographs and deep learning algorithm requires further exploration [39].

(2) Uncertainty in grassland class variation

Our results indicated that the spatial distribution pattern of grassland classes in Inner Mongolia has changed greatly (30.98% of overlapped grassland) since the 1980s. On the one hand, the grassland class variation may be caused by climate change and human activities in the past 40 years [11,12,14]. On the other hand, the grassland coverage of this study was derived from MCD12Q1 land-over production in 2019, while the coverage of the 1980s came from field measurement [20]. There was a large difference between each other. Moreover, the overall accuracy of the optimum classification method was 76.92% (Table 4).

(3) Approach for improving the accuracy of classification in the future

The characteristics of growth season NDVI have been commonly used as the classification indices for grassland classification [30–32,36,37]. However, the structure and growth of grassland vegetation were also affected by climate (illumination time, temperature, and precipitation), soil (fertilization and texture), topography (elevation and slope), management factors (fencing and grazing), and so on [29,33,40,53–55]. There were still large errors and uncertainties in grassland class mapping by using NDVI simply [39]. Pan et al. (2003) [56] indicated that integrating the climate, terrain, and spectral data can improve the accuracy of vegetation-type classification by 8.1% compared with that derived only from multitemporal NDVI images. Ma (2015) [57] indicated that integrating the spectral indices and terrain factors can improve the accuracy of alpine grassland classification, with OA increased by 25.3% to 30.4% compared with that derived only based on spectral indices. Hence, future studies can explore the method of combining machine learning algorithms and multitype indices (i.e., NDVI, DEM, temperature, precipitation, and so on) to improve the accuracy of grassland classification [58]. At the same time, the spatial–temporal dynamic variation of grassland classes is more easily monitored with a long time series of input data [3,59]. Although the RF algorithm achieves higher accuracy than the other methods, the training process and the equations of the RF algorithm cannot be observed; therefore, the internal mechanisms of this model cannot be easily explained. In a future work, we plan to compare the advantages and disadvantages of different machine learning algorithms (ANN, SVM, and RF) to establish the best classification method.

5. Conclusions

This study examined four classification methods and evaluated their accuracy based on characteristic indices of NDVI in the growing season and UAV field observation. Then, the spatial distribution of grassland classes was compared with that generated in the 1980s. Our results showed that the sum, maximum, and mean of NDVI from July to September have a higher importance value for grassland classification, while the range, standard deviation, and minimum of NDVI from May to September have a lower importance value. The RF algorithm can effectively classify the grassland classes in Inner Mongolia with an overall accuracy of 72.17%. Compared with the grassland class mapped in the 1980s (overlapped area), 30.98% of the grassland classes have been changed. Our study demonstrated that it was feasible to map the grassland class at large scales using satellite remote sensing, UAV surveying, and machine learning methods. In a future work, multitype indices, including remote sensing indices, climates, topography, and soil, are required to improve the grassland classification.

Supplementary Materials: The following are available online at https://www.mdpi.com/article/10.3390/rs14092094/s1. Table S1: Scheme of land cover types reclassification.

Author Contributions: B.M. and S.Y. designed this study; B.M., Y.Z., Z.Y., Y.L., M.L., Y.S., H.Y. (Huilin Yu) and J.Z. were responsible for the field observation, data processing, analysis, and writing of the paper; J.C., H.Z., J.L. (Jie Lian), M.H., J.L. (Jinrong Li), H.Y. (Hongyan Yu) and L.C. were responsible for the field observation. S.Y. made valuable revisions and editing of the paper. All authors have read and agreed to the published version of the manuscript.

Funding: The Planned Science-Technology Project of Inner Mongolia, China (2021GG0050); the National Natural Science Foundation of China (41801102); and the IWHR Research and Development Support Program (MK0199A122021).

Acknowledgments: The authors thank Yuting Huang for helping with the experiments, the Naiman Desertification Research Station, and the Cold and Arid Regions Environmental and Yinshanbeilu Grassland Ecohydrology National Observation and Research Station for their help in the field observation. We also appreciate the editor's and reviewers' constructive suggestions to greatly improve the paper.

Conflicts of Interest: The authors declare no conflict of interest.

References

1. Ren, J.Z.; Hu, Z.Z.; Zhao, J.; Zhang, D.G.; Hou, F.J.; Lin, H.L.; Mu, X.D. A grassland classification system and its application in China. *Rangeland J.* **2008**, *30*, 199–209. [CrossRef]
2. Jacobsen, A.; Nielsen, A.A.; Ejrnæs, R.; Groom, G.B. Spectral identification of danish grassland classes related to management and plant species composition. In Proceedings of the 4th International Airborne Remote Sensing Conference and Exhibition/21st Canadian Symposium on Remote Sensing, Ottawa, ON, Canada, 21–24 June 1999; pp. 74–81.
3. Lin, H.L.; Feng, Q.S.; Liang, T.G.; Ren, J.Z. Modelling global-scale potential grassland changes in spatio-temporal patterns to global climate change. *Int. J. Sustain. Dev. World. Ecol.* **2013**, *20*, 83–96. [CrossRef]
4. Pratt, D.J.; Greenway, P.J.; Gwynne, M.D. A Classification of East African Rangeland, with an Appendix on Terminology. *J. Appl. Ecol.* **1966**, *3*, 369–382. [CrossRef]
5. Lauenroth, W.K. Grassland Primary Production: North American Grasslands in Perspective. In *Perspectives in Grassland Ecology*; Springer: New York, NY, USA, 1979; pp. 3–24.
6. Wei, Y.X.; Chen, Q.G. Grassland classification and evaluation of grazing capacity in Naqu Prefecture, Tibet Autonomous Region, China. *N. Z. J. Agric. Res.* **2001**, *44*, 253–258.
7. Cui, X.; Guo, Z.G.; Liang, T.G.; Shen, Y.Y.; Liu, X.Y.; Liu, Y. Classification management for grassland using MODIS data: A case study in the Gannan region, China. *Int. J. Remote Sens.* **2012**, *33*, 3156–3175. [CrossRef]

8. Hu, Z.W.; Zhang, S.; Yu, X.Y.; Wang, X.S. Preliminary Research on Grassland Fine-classification Based on MODIS. *IOP Conf. Ser. Earth Environ. Sci.* **2014**, *17*, 012079. [CrossRef]
9. Ren, H.G.; Zhou, G.S. Measuring the impacts of anthropogenic activities on Inner Mongolian temperate grassland. *Land Degrad Dev.* **2018**, *29*, 2942–2950. [CrossRef]
10. Guo, D.; Song, X.N.; Hu, R.H.; Cai, S.H.; Zhu, X.M.; Hao, Y.B. Grassland type-dependent spatiotemporal characteristics of productivity in Inner Mongolia and its response to climate factors. *Sci. Total Environ.* **2021**, *775*, 145644. [CrossRef]
11. Su, Y.J.; Guo, Q.H.; Hu, T.Y.; Guan, H.C.; Jin, S.C.; An, S.Z.; Chen, X.L.; Guo, K.; Hao, Z.Q.; Hu, Y.M.; et al. An updated Vegetation Map of China (1:1,000,000). *Sci. Bull.* **2020**, *65*, 1125–1136. [CrossRef]
12. Miao, L.J.; Sun, Z.L.; Ren, Y.J.; Schierhorn, F.; Müller, D. Grassland greening on the Mongolian Plateau despite higher grazing intensity. *Land Degrad Dev.* **2020**, *32*, 792–802. [CrossRef]
13. Su, L.D.; Yang, J.; Wang, Z.Q.; Gu, R.; Yan, Y.L.; Gao, Q.Z. Climate change and its impacts on distribution pattern of grassland types in Inner Mongolia. *Chin. J. Agrometeorol.* **2015**, *36*, 139–148.
14. Wei, P.; Xu, L.; Pan, X.B.; Hu, Q.; Li, Q.Y.; Zhang, X.T.; Shao, C.X.; Wang, C.C.; Wang, X.X. Spatio-temporal variations in vegetation types based on a climatic grassland classification system during the past 30 years in Inner Mongolia, China. *CATENA* **2020**, *185*, 104298. [CrossRef]
15. Su, R.N.; Yu, T.; Dayananda, B.; Bu, R.; Su, J.H.; Fan, Q.Y. Impact of climate change on primary production of Inner Mongolian grasslands. *Glob. Ecol. Conserv.* **2020**, *22*, e00928. [CrossRef]
16. Naidoo, R.; Hill, K. Emergence of indigenous vegetation classifications through integration of traditional ecological knowledge and remote sensing analyses. *Environ. Manag.* **2006**, *38*, 377–387. [CrossRef] [PubMed]
17. Ichter, J.; Evans, D.; Richard, D. *Terrestrial Habitat Mapping in Europe: An Overview*; European Environmental Agency: Luxembourg, 2014; p. 152.
18. De Cáceres, M.; Wiser, S.K. Towards consistency in vegetation classification. *J. Veg. Sci.* **2012**, *23*, 387–393. [CrossRef]
19. Tierney, D.A.; Fletcher, A.T.; Erskine, P.D. Standard survey designs drive bias in the mapping of upland swamp communities. *Austral. Ecol.* **2015**, *40*, 782–793. [CrossRef]
20. 1:1,000,000 China Grassland Resource Mapping Committee. *1:1 Million Atlas of Grassland Resources in China*; China Cartographic Publishing House: Beijing, China, 1993.
21. Meiss, M.; Jacob, F.; Duveiller, G. Remote sensing for agricultural applications: A meta-review. *Remote Sens. Environ.* **2020**, *236*, 111402.
22. Jamshidi, S.; Zand-Parsa, S.; Niyogi, D. Assessing Crop Water Stress Index of Citrus Using In-Situ Measurements, Landsat, and Sentinel-2 Data. *Int. J. Remote Sens.* **2021**, *42*, 1893–1916. [CrossRef]
23. Jahromi, M.N.; Jahromi, M.N.; Pourghasemi, H.R.; Zand-Parsa, S.; Jamshidi, S. Accuracy assessment of forest mapping in MODIS land cover dataset using fuzzy set theory. In *Forest Resources Resilience and Conflicts*; Elsevier: Amsterdam, The Netherlands, 2021; pp. 165–183.
24. Reinermann, S.; Asam, S.; Kuenzer, C. Remote Sensing of Grassland Production and Management—A Review. *Remote Sens.* **2020**, *12*, 1949. [CrossRef]
25. Masoud, M.; Bahram, S.; Mohammad, R.; Fariba, M.; Zhang, Y. Very Deep Convolutional Neural Networks for Complex Land Cover Mapping Using Multispectral Remote Sensing Imagery. *Remote Sens.* **2018**, *10*, 1119.
26. Wulder, M.A.; Coops, N.C.; Roy, D.P.; White, J.C.; Hermosilla, T. Land cover 2.0. *Int. J. Remote Sens.* **2018**, *39*, 4254–4284. [CrossRef]
27. Dixon, A.P.; Faber-Langendoen, D.; Josse, C.; Morrison, J.; Loucks, C.J. Distribution mapping of world grassland types. *J. Biogeogr.* **2014**, *41*, 2003–2019. [CrossRef]
28. Meng, B.P.; Ge, J.; Liang, T.G.; Yang, S.X.; Gao, J.; Feng, Q.S.; Cui, X.; Huang, X.D.; Xie, H.J. Evaluation of Remote Sensing Inversion Error for the Above-Ground Biomass of Alpine Meadow Grassland Based on Multi-Source Satellite Data. *Remote Sens.* **2017**, *9*, 372. [CrossRef]
29. Meng, B.P.; Liang, T.G.; Yi, S.H.; Yin, J.P.; Cui, X.; Ge, J.; Hou, M.J.; Lv, Y.Y.; Sun, Y. Modeling alpine grassland above ground biomass based on remote sensing data and machine learning algorithm: A case study in the east of Tibetan Plateau, China. *IEEE J. Sel. Top. Appl. Earth Obs. Remote Sens.* **2020**, *13*, 2986–2995. [CrossRef]
30. Wen, Q.K.; Zhang, Z.X.; Liu, S.; Wang, X.; Wang, C. Classification of Grassland Types by MODIS Time-Series Images in Tibet, China. *IEEE J. Sel. Top. Appl. Earth Obs. Remote Sens.* **2010**, *3*, 404–409. [CrossRef]
31. Zhang, X.M.; Sheng, Y.; Nan, Z.T.; Zhao, L.; Zhou, G.Y.; Yue, G.Y. Vegetation classification of alpine grassland based on decision tree approach in the Wenquan area of the Qinghai-Tibet Plateau. *Pratacult. Sci.* **2011**, *28*, 2074–2083.
32. Zhang, X.S. Vegetation Classification Research of Grassland Based on Decision Tree Approach in Xinjiang Yili Area. Master's Thesis, Lanzhou Jiaotong University, Lanzhou, China, 2015.
33. Liang, T.G.; Yang, S.X.; Feng, Q.S.; Liu, B.K.; Zhang, R.P.; Huang, X.D.; Xie, H.J. Multi-factor modeling of above-ground biomass in alpine grassland: A case study in the Three-River Headwaters Region, China. *Remote Sens. Environ.* **2016**, *186*, 164–172. [CrossRef]
34. Yi, S.H. FragMAP: A tool for long-term and cooperative monitoring and analysis of small-scale habitat fragmentation using an unmanned aerial vehicle. *Int. J. Remote Sens.* **2017**, *38*, 8–10. [CrossRef]
35. Yi, S.H.; Chen, J.J.; Qin, Y.; Xu, G.W. The burying and grazing effects of plateau pika on alpine grassland are small: A pilot study in a semiarid basin on the Qinghai-Tibet Plateau. *Biogeosciences* **2016**, *13*, 6273. [CrossRef]

36. Wang, Z.X.; Liu, C.; Zhao, B.R. Potentials and limitation of AVHRR for grassland classification in Xilingol, Inner Mongolia. *J. Nat. Resour.* **2003**, *18*, 704–711.
37. Zhao, B.R.; Liu, C.; Liu, A.J.; Wang, Z.X. Estimate the yield of grassland using MODIS-NDV—A case study of the grassland in Xilinguole in Inner Mongolia. *Pratacult. Sci.* **2004**, *21*, 12–15.
38. Navin, M.S.; Agilandeeswari, L. Comprehensive review on land use/land cover change classification in remote sensing. *J. Spectr. Imaging* **2020**, *9*, a8. [CrossRef]
39. Meng, B.P.; Yang, Z.G.; Yu, H.Y.; Qin, Y.; Sun, Y.; Zhang, J.G.; Chen, J.J.; Wang, Z.W.; Zhang, W.; Li, M.; et al. Mapping of Kobresia pygmaea Community Based on Umanned Aerial Vehicle Technology and Gaofen Remote Sensing Data in Alpine Meadow Grassland: A Case Study in Eastern of Qinghai–Tibetan Plateau. *Remote Sens.* **2021**, *13*, 2483. [CrossRef]
40. Meng, B.P.; Gao, J.L.; Liang, T.G.; Cui, X.; Ge, J.; Yin, J.P.; Feng, Q.S.; Xie, H.J. Modeling of Alpine Grassland Cover Based on Unmanned Aerial Vehicle Technology and Multi-Factor Methods: A Case Study in the East of Tibetan Plateau, China. *Remote Sens.* **2018**, *10*, 320. [CrossRef]
41. Sun, Y.; Yi, S.H.; Hou, F.J. Unmanned aerial vehicle methods makes species composition monitoring easier in grasslands. *Ecol. Indic.* **2018**, *95*, 825–830. [CrossRef]
42. Friedl, M.A.; Brodley, C.E. Decision tree classification of land cover from remotely sensed data. *Remote Sens. Environ.* **1997**, *61*, 399–409. [CrossRef]
43. Chen, T.; Zhu, L.; Niu, R.Q.; Trinder, C.J.; Peng, L.; Lei, T. Mapping landslide susceptibility at the Three Gorges Reservoir, China, using gradient boosting decision tree, random forest and information value models. *J. Mt. Sci.* **2020**, *17*, 670–685. [CrossRef]
44. Breiman, L. Bagging predictors. *Mach. Learn.* **1996**, *24*, 123–140. [CrossRef]
45. Breiman, L. Random Forests. *Mach. Learn.* **2001**, *45*, 5–32. [CrossRef]
46. Dreiseitl, S.; Ohno-Machado, L. Logistic regression and artificial neural network classification models: A methodology review. *J. Biomed. Inform.* **2002**, *35*, 352–359. [CrossRef]
47. Tiryaki, S.; Aydın, A. An artificial neural network model for predicting compression strength of heat treated woods and comparison with a multiple linear regression model. *Constr. Build. Mater.* **2014**, *62*, 102–108. [CrossRef]
48. Yang, S.; Feng, Q.; Liang, T.; Liu, B.; Zhang, W.; Xie, H. Modeling grassland above-ground biomass based on artificial neural network and remote sensing in the Three-River Headwaters Region. *Remote Sens. Environ.* **2017**, *204*, 448–455. [CrossRef]
49. Yu, K.F.; Lehmkuhl, F.; Falk, D. Quantifying land degradation in the Zoige Basin, NE Tibetan Plateau using satellite remote sensing data. *J. Mt. Sci.* **2017**, *14*, 77–93. [CrossRef]
50. Zhang, J.G.; Liu, D.W.; Meng, B.P.; Chen, J.J.; Wang, X.Y.; Jiang, H.; Yu, Y.; Yi, S.H. Using UAVs to assess the relationship between alpine meadow bare patches and disturbance by pikas in the source region of Yellow River on the Qinghai-Tibetan Plateau. *Glob. Ecol. Conserv.* **2021**, *26*, e01517. [CrossRef]
51. Lv, Y.; Shen, M.; Meng, B.; Zhang, H.; Sun, Y.; Zhang, J.; Chang, L.; Li, J.; Yi, S. The Similarity between Species Composition of Vegetation and Soil Seed Bank of Grasslands in Inner Mongolia, China: Implications for the Asymmetric Response to Precipitation. *Plants* **2021**, *10*, 1890. [CrossRef] [PubMed]
52. Zhang, X.K.; Lu, X.Y.; Wang, X.D. Spatial-Temporal NDVI Variation of Different Alpine Grassland Classes and Groups in Northern Tibet from 2000 to 2013. *Mt. Res. Dev.* **2015**, *35*, 254–263. [CrossRef]
53. Gao, T.; Yang, X.C.; Jin, Y.X.; Ma, H.L.; Li, J.Y.; Yu, H.D.; Yu, Q.Y.; Zheng, X.; Xu, B. Spatio-Temporal Variation in Vegetation Biomass and Its Relationships with Climate Factors in the Xilingol Grasslands, Northern China. *PLoS ONE* **2013**, *8*, e83824. [CrossRef]
54. Liu, M.; Liu, G.H.; Gong, L.; Wang, D.B.; Sun, J. Relationships of Biomass with Environmental Factors in the Grassland Area of Hulunbuir, China. *PLoS ONE* **2014**, *9*, e102344. [CrossRef]
55. Li, Z.Q.; Guo, X.L. Topographic effects on vegetation biomass in semiarid mixed grassland under climate change using AVHRR NDVI data. *Br. J. Environ. Clim. Chang.* **2014**, *4*, 229–242. [CrossRef]
56. Pan, Y.; Li, X.; Gong, P.; He, C.; Shi, P.; Pu, R. An integrative classification of vegetation in China based on NOAA AVHRR and vegetation-climate indices of the Holdridge life zone. *Int. J. Remote Sens.* **2003**, *24*, 1009–1027. [CrossRef]
57. Ma, W.W. *Study on Methods for Grassland Classification and Quality Estimation by Remote Sensing: A Case Study in the Region around Qinghai Lake*; University of Chinese Academy of Sciences: Beijing, China, 2015.
58. Guo, Q.H.; Guan, H.C.; Hu, T.Y.; Jin, S.C.; Su, Y.J.; Wang, X.J.; Wei, D.J.; Ma, Q.; Sun, Q.H. Remote sensing-based mapping for the new generation of Vegetation Map of China (1:500,000). *Sci Sin Vitae* **2021**, *51*, 229–241. (In Chinese) [CrossRef]
59. Feng, Q.S.; Liang, T.G.; Huang, X.D.; Lin, H.L.; Xie, H.J.; Ren, J.Z. Characteristics of global potential natural vegetation distribution from 1911 to 2000 based on comprehensive sequential classification system approach. *Grassl. Sci.* **2013**, *59*, 87–99. [CrossRef]